First-principles study of grain-boundary wetting in Fe-Σ5(013)[100] tilt boundary

T. Auger [a,*], L.L. Wang [b], Duane D. Johnson [b,c], X. Gong [d,*]

[a] *PIMM/Arts et Métiers Institute of Technology, CNRS (UMR 8006), CNAM, 151 bd de l'hôpital, Paris 75013, France*

[b] *Ames National Laboratory, U.S. Department of Energy, Ames, IA 50011, USA*

[c] *Department of Materials Science & Engineering, Iowa State University, Ames, IA 50011, USA*

[d] *Advanced Nuclear Energy Research Team, Department of Nuclear Science and Technology, College of Physics and Optoelectronic Engineering, Shenzhen University, Shenzhen 518060, China*

ABSTRACT

We report an ab-initio study of grain-boundary wetting (GBW) in three systems (Fe/Zn, Fe/Pb & Fe/Bi) on a Σ5 (013)[100] tilt grain boundary. An energy-based approach is pursued and adapted to the study of liquid-metal/solid-metal interfaces. We provide a sound calculation of the wettability parameter S (i.e., defined as the minimum energy difference between the unbroken initial state and final state with liquid-metal/solid-metal interfaces). Solid/liquid interfaces are modelled by ab-initio molecular dynamics, also allowing a study of structural effects in the liquid phase near the solid interface. We show how surface energies for solid-metal/liquid-metal interfaces need a special treatment for the liquid-metal chemical potential due to the change in crystallinity near the interface. The computation of the wettability criterion for the three systems correctly predicts the GBW trend known experimentally for these systems. The computations are compared with small-scale TEM experiments on GBW of two systems (Fe/Pb and Fe/Bi) and it is shown to provide reasonable results. This approach offers new perspectives in predicting GBW trends across various systems.

1. Introduction

Grain boundaries (GB) of metallic polycrystalline materials can suffer from grain-boundary wetting (GBW) when in contact with low melting point liquid metals [1]. This is observed in several binary systems where the polycrystalline solid phase evolves spontaneously towards the replacement of grain boundaries with an intergranular film of liquid metal of nanometer-sized thickness. The nanoscale intergranular layer spontaneously forms as a first wetting step before eventually becoming much larger by dissolution diffusion phenomena. Another process where one observes GBW is by alloying several elements (often immiscible) followed by high-temperature annealing above the disordering or phase decomposition temperature [2]. After thermal annealing, the thermodynamic equilibrium state is reached with GB segregation of impurities or as a complexion of the GB [3]. Generally, when GBW occurs, in some cases above a transition temperature, it leads to detrimental mechanical properties with brittle fracture at the intergranular film. The known couples are Al/Sn, Cu/In, Al/Pb-Sn, Al/Ga, Al/Sn-Ga, Cu/Bi, Fe-Si/Zn, Mo/Ni, W/Ni, Zn/Sn and Ni/Bi [1,2]. The

kinetics of such spontaneous processes can be truly astounding with GB penetration speed reaching hundreds of micrometers per second in the Al/Ga case or leading to disastrous brittle fracture or complete ruin of an otherwise ductile material like Cu/Bi [4,5]. With ferromagnetic bcc alloys, a well-known case of GBW is Fe-5 %Si/Zn above 650 °C [6]. At the same time, GBW does not spontaneously occur in other systems such as Fe/Pb [7]. No experimental data has been reported up to now on the Fe/Bi couple. Instead these former systems when tested against liquid-metal embrittlement (LME) require additional mechanical strain in order to fracture in a brittle manner at grain boundaries; it is then not proven that GBW systematically plays a role in LME in particular for that class. The conventional analysis behind this major difference in GB wettability behavior is supposed to be captured by the energetics of the interface being driven towards GBW if energetically favorable, while the classical LME behavior only occurs as a result of the reduction of cohesion by adsorption of liquid metal at the crack tip [8]. In the GBW case, transport of liquid species precedes as a requirement or as an aggravating factor for LME.

Wettability of interfaces is classically described energetically using

---

the energy difference between the final (broken) and initial (unbroken) states [9]. For partial wetting, the deviation from equilibrium is a relevant measure of the driving force of the liquid spreading evolution [10]. For the GBW process, the quantity of interest is the wettability parameter, which is denoted as S and defined as the energy difference between two times the solid-liquid surface energy (eventually depending upon the liquid metal chemical potential) and the GB energy, i.e.:

$$S(\mu_{LM}) = 2\gamma_{SL}^{Fe-LM}(\mu_{LM}) - \gamma_{GB} \qquad (1)$$

In case of a negative energy difference ($S<0$), the system should evolve towards the formation of an intergranular film characterized by two solid-liquid interfaces, i.e., a GBW transition. For a positive energy difference ($S>0$), the GB is deemed more favorable energetically. In such case, the solid-liquid system should not evolve from an initial state characterized by a triple line and the GB is to remain bonded unless one provides sufficient mechanical strain energy to allow for a brittle fracture dissipation induced by adsorption (i.e. standard LME process).

The major difficulty in studying this issue is to correctly assess solid-liquid interfaces at the atomic level (on the structural as well as energetical point of view). Experimentally it is not feasible to assess the solid-liquid interfacial energetics for all the systems that one would like to be able to investigate, with a few exceptions like aluminum-based systems [11]. Indeed, one could turn towards wetting studies on a surface by the sessile drop technique to measure solid-liquid energetics, but this does not allow the investigation of systems showing total wetting. In that case, only an upper solid-liquid interfacial energy limit can be inferred, due to the absence of a triple junction with a non-null Young's angle. Therefore, only partial wetting cases can in principle be interpreted.

Modelling a solid-liquid interface by ab-initio simulations is therefore a reasonable alternative. The systems of interest here are chosen to give unequivocal response. In this respect, describing GBW or its non-occurrence is very desirable as it would validate the ability of ab-initio methods to predict these behaviors (at least when extrapolated at 0 K). This requires one to model the solid/liquid interfaces by ab-initio molecular dynamics (AIMD) in a first step, then also allowing a study of structuring effects in the liquid phase in the vicinity of a solid surface.

Studying the liquid structure by AIMD (static or dynamic properties) is a well-established technique where Pb and Bi for example have been modelled since the nineties [12,13]. AIMD has been shown to be able to reproduce several important experimental features of the liquid dynamics (structural and electronic levels) [14]. Pb and Zn are considered as simple liquids with a conventional molecular behavior. On the other hand, Bi has a complex molecular structure in the liquid state with either a double structure [15] or a remnant from a Peierls' instability even in the liquid state [16].

For such purpose, the selected systems are the Fe/Zn, Fe/Pb and Fe/Bi binaries. The Fe/Zn system has a clear GBW transition above 650 °C, which is of concern in industrial context for welding of galvanized steel sheets [6]. On the other hand, experiments indicate that the Fe/Pb binary (and supposedly also Fe/Bi) does not display such spontaneous transition [7], while Fe can be strongly embrittled by liquid Pb under tensile loading [17]. In the context of the established LME concern for Fe/Pb-Bi systems, the question of their GBW trend is of prime importance.

An ab-Initio study is here carried out of liquid-metal (LM)/solid-metal (SM) interfaces (Fe(013)/LM) in the three systems (Fe/Zn, Fe/Pb & Fe/Bi). An energetic approach of GBW is then pursued and adapted for a Σ5(013)[100] tilt GB in iron taken an example of a general GB. The calculation of the wettability parameters S for each system is pursued and a subsequent discussion of GBW is carried out.

2. Computational details

The first-principles scheme utilized to model solid-liquid interfaces uses AIMD and total-energy calculations within the density functional theory (DFT) framework, as implemented in the Vienna Atomic Simulation Package (VASP, version 5.4.4) [18–20] using plane-wave basis set and projector-augmented wave (PAW) pseudo-potentials, within a Generalized-Gradient Approximation (GGA) via the PBE exchange-correlation functional [21]. The Monkhorst-Pack scheme was systematically used for k-point sampling of the Brillouin zone [22]. The cutoff energy for plane-wave basis was set to 520 eV for all calculations. The electronic minimizations were carried out using a first-order Methfessel-Paxton smearing of 0.05 eV [23]. Extra valence electron d-states were included for Pb ($5d^{10}6s^26p^2$) and Bi ($5d^{10}6s^26p^3$), while the standard electronic configuration was used for Zn ($3d^{10}4s^2$) and Fe ($3d^74s^1$). Spin-polarized calculations were used for all calculations. For each supercell, the correct alignment of Fe spins (ferromagnetic state) was checked at every MD step (relaxation and final convergence).

The ground states for the elements considered in this work (Fe, Pb, Bi and Zn) as modelled by DFT-GGA are reported in the table below. Our results are consistent with previous studies for these elements [24–26]. For Bi, not including the spin-orbit (SO) coupling is known not to affect charge density computations and therefore it was not included in computations with heavy elements [25]. Including SO effects for Pb largely reduces the difference between the experimental measurement and the first-principles value of cohesive energy [26]. It does not affect the surface energies computations.

To model a solid-liquid interface one runs an AIMD simulation of the liquid in a slab geometry in contact with an iron solid surface at high temperature. Several liquid-like configurations can then be generated to be used as a starting point for further structural relaxation. The GB chosen here is a Σ5[100](013) Coincident Site Lattice (CSL) type GB (symmetric tilt of 36.8° around <001>). Therefore, an iron {013} surface was chosen to face the liquid phase. It is taken to be representative of a general GB from the energy point of view. The configuration allowing to model a solid-liquid interface is a liquid layer sandwiched between an iron slab with a normal along a <013> direction. 20 layers of six iron atoms (so a total M of 120 iron atoms) are used in an orthorhombic supercell of 0.849 nm x 0.895 nm x 3.579 nm size (axis oriented along [1–30], [00–1] and [310] directions) with periodic boundary conditions. The number of liquid atoms (hereafter N atoms) is adjusted for each liquid metal so as to reach a density close to the equilibrium one as well as ensuring that the external pressure after relaxation remains below 5 kBar. With this constraint, the Fe/Pb supercell, in addition to Fe atoms, contains 40 Pb atoms while the Fe/Bi one contains 36 Bi atoms and the Fe/Zn one contains 86 Zn atoms. The supercell transverse size allows for a liquid channel nearly 1.8 nm thick (a "nano-channel").

The calculation sequence is the following: First, up to 60 ps of total MD time with a 5 fs time step were simulated for each system using a Nosé thermostat to regulate the temperature at 1000 K. All the atoms of Fe are held fixed during the MD run. Only the gamma point is used to sample the Brillouin zone at this stage. The average force felt by each atom, the energy, pressure and the temperature are recorded at every step to be able to select a configuration labelled as a "liquid" configuration. So, at a late time of the MD simulation, where the effect of the initial configuration is deemed erased, a supercell configuration is selected based upon a force (local minimum of the average force felt by all atoms) or an energy criterion (local minimum of the cell energy) with simultaneously a low pressure within the supercell.

Second, relaxation of the supercell towards fully relaxed forces (average force < 0.02 eV/Å^{-1}) is carried out while checking that the external pressure remains lower than 5 kBar (This is the criterion that was used to select the number of liquid-metal atoms in the supercell). The 12 inner layers of (013) of Fe are held fixed at the equilibrium Fe unit cell while 4 outer layers of Fe are allowed to relax at each interface (periodic boundary conditions ensure that there are two solid-liquid interfaces in the cell). The k-points mesh used to relax is $4 \times 4 \times 1$. Some initial configurations led to a full recrystallization of the liquid during relaxation, so they were further disregarded and the process

repeated with another starting configuration until a satisfying structural configuration exempt from a full crystallization was obtained. Lastly, upon structural relaxation convergence, a final calculation is carried out using a finer k-points mesh ($8 \times 8 \times 2$) to ensure that the energy calculation (E_0) is well k-point converged.

The solid-liquid interface energy (in J/m^2) is then obtained as a function of the chemical potentials (M Fe atoms and N liquid-metal atoms) in the following way:

$$\gamma_{SL}^{Fe-ML}(\mu_{LM}) = \frac{1}{2A}(E_0 - M\mu_{Fe} - N\mu_{LM}) \tag{2}$$

with $A = 0.759855$ nm^2 (0.849 nm x 0.895 nm), $M = 120$. E_0 is the converged cell energy, the iron chemical potential is taken from the bulk state. The chemical potential to be considered for the liquid metal is estimated by comparing the crystalline state versus a "liquid" or amorphous-like state. Here the strategy is to calculate the range of chemical potential spanned by a transition from the crystalline state to an amorphous one. This is justified as the liquid state evolves from a layered structure close to the iron (310) surface compared to a more amorphous structural organization a few layers away from it. This leads to a dependence of surface energies to the chemical potential between these two extreme cases. The discussion on grain-boundary wetting will be led using the same approach.

3. Experimental grain-boundary wetting analysis for Fe-Bi cast alloy

Estimates of the solid-liquid interfacial energy are available for Fe/Zn and Fe/Pb. For Fe/Zn, based on fit of the hydrostatic pressure dependence of GBW and estimates by Miedema et al., it has been considered that $\gamma_{SL} \approx 0.3 \pm 0.1 \frac{J}{m^2}$ [27]. For Fe/Pb, using annealed Fe/Pb (873 K) sintered powder samples data observed by TEM [7], it has been evaluated using the dihedral angle technique at $\gamma_{SL} \approx 1.2 \frac{J}{m^2}$ [28]. To provide for an experimental estimate of the solid-liquid interface energy for the remaining system of interest here (i.e., Fe/Bi), the methodology of studying the equilibrium dihedral angle at a junction between a grain boundary and a liquid inclusion was pursued similarly to previous studies [7,28]. An Fe-10wt% Bi alloy was prepared by vacuum-induction melting. The residual oxygen in the ingot was measured to be 0.001248wt%. A small sample was cut from the ingot and then sealed in a quartz tube under high vacuum, followed by annealing in a furnace at 350 °C for 2 h (above the melting temperature of bismuth). Afterwards, the tube was taken from the furnace and immediately threw into ice water to quench the sample. The triple junction at a random GB in contact with an inclusion of bismuth was characterized by FIB machining of TEM lamella (see supplementary). The dihedral wetting angle at a random GB was consistently measured at 102° for three triple lines.

4. Results

4.1. Liquid structure

The purpose of investigating the liquid structure is twofold. One would like first to check that the liquid phase can be simulated properly. One criterion is that the pair distribution function should be reasonably reproduced giving access to realistic configurations in the liquid phase by the modelling scheme. Second, one needs to reasonably estimate the range of chemical potential to consider an estimate of solid-liquid interface energy. For such purpose, realistic configurations need to be modelled and used to define this energy. The liquid structure was investigated for Bi and Pb using a cubic supercell ($1.666 \times 1.666 \times 1.666$ nm^3 for Bi and $1.6 \times 1.6 \times 1.6$ nm^3 for Pb) filled with 125 atoms (Bi or Pb, respectively) in periodic boundary conditions. A cubic supercell ($1.165 \times 1.165 \times 1.165$ nm^3) with 100 atoms was used for Zn.

The corresponding density is 9.384 g·cm^{-3} for liquid Bi as compared with an experimental density of 9.87 g·cm^{-3} at 700 K, while the corresponding density is 10.503 g·cm^{-3} for liquid Pb as compared with an experimental density of 10.5 g·cm^{-3} at 700 K. For liquid Zn the corresponding density is 6.69 g·cm^{-3} (compared with a 6.87 g·cm^{-3} experimental density at 723 K). The AIMD was carried out in the canonical ensemble (NVT) with a Nosé-Hoover thermostat. The static properties are investigated via the pair distribution function that is computed over the supercell for N atoms using the following expression:

$$\rho_0 g(r) = \frac{1}{N}\left\langle \sum_i \sum_j \delta\{\boldsymbol{r} - (\boldsymbol{r}_i - \boldsymbol{r}_j)\}\right\rangle - \delta(r) \tag{3}$$

where ρ_0 is the average number density. The coordination number for number of first neighbors is then computed classically using:

$$n_1 = \int_0^{r_{min}} 4\pi\rho_0 g(\boldsymbol{r})dr \tag{4}$$

The AIMD reproduces fairly well the pair distribution functions as measured by x-ray diffraction (Fig. 1a for liquid Bi, Fig. 1b for liquid Pb and Fig. 1c for liquid Zn) [30]. In the AIMD, the first-neighbor peak distance is found at 0.334 nm for Pb, 0.319 nm for Bi and 0.253 nm for Zn. Previous work by AIMD found similar first-neighbor peak distance [19]. Experimentally, the first-neighbor peak is measured at 0.33 nm for Pb [30], at 0.325 nm for liquid Bi [29] and 0.26 nm for liquid Zn [30].

For Pb, the agreement is quite good with a first-neighbor coordination number approaching 11, characteristic of a simple liquid. A similar conclusion is reached for liquid Zn, where the AIMD coordination number of 11.5 also signals a simple liquid. For Bi, a shoulder is observed on the right side from the first peak as reported by many previous experiments [14]. The first-neighbor coordination number found for Bi is between 7 and 7.5 ($r_{max} = 0.405$ nm). Our modelling of liquid Bi compares well with previous AIMD modelling [14]. The shoulder in the pair distribution function of Bi is indicative of the fact that Bi is not a simple liquid but belongs to the class of complex liquids with structural order. The liquid description is therefore sufficient to allow a calculation of the chemical potential of "liquid" Bi, Pb or Zn species.

A liquid configuration with low average force as well as low internal cell pressure was selected and further relaxed using a conjugate gradient algorithm. The Brillouin zone was sampled using a $3 \times 3 \times 3$ k-points grid. The convergence criterion was all force amplitudes lying below 0.02 eV·Å^{-1} threshold. Some trials resulted in recrystallization. When such an evolution was detected, the configuration was no longer considered and disregarded. A final higher density Brillouin zone sampling ($7 \times 7 \times 7$ k-points) was carried out to ensure that convergence is reached within 1 meV.

These results can be used to qualitatively estimate the heat of fusion of each of these three elements in a rudimentary approach. Table 2 summarizes the calculations: one can see a relatively good agreement for the enthalpy of fusion for Pb and Bi. The agreement is less good for Zn but remains acceptable.

4.2. Solid-liquid interfaces

Fig. 2a–2c show the projected atomic-density profile for Fe/Pb, Fe/Bi and Fe/Zn interfaces respectively as given by the following:

$$\rho(z) = \frac{\langle N_z \rangle}{L_x L_y \Delta z} \tag{5}$$

where $\langle N_z \rangle$ is the time average of the number of particles between z and $z+\Delta z$. L_x and L_y are lateral sizes of the simulation box.

The narrow peaks on the right-hand side come from the rigid position of Fe atoms. On the left-hand side of the plot, one observes the density
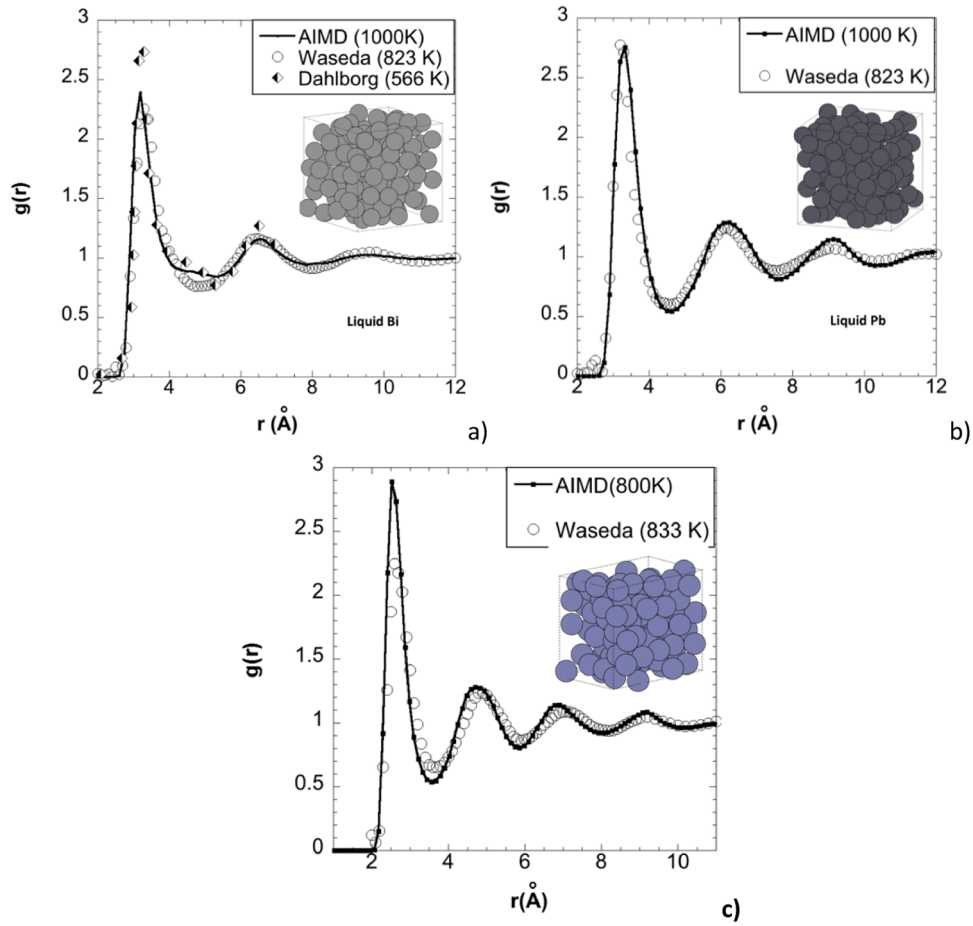
Fig. 1. AIMD-derived pair distribution function g(r) for the liquid state: (a) Bi at 1000 K compared with x-ray data from Dahlborg (at 566 K) [29] and Waseda (at 577 K) [30]; (b) Pb at 1000 K compared with x-ray data from Waseda (at 823 K) [30]; (c) Zn at 800 K compared with x-ray data from Waseda (at 833 K) [30]. A sample configuration is shown in insert. (color online).

fluctuations of the liquid (symmetric due to the two Fe(013) interfaces). Near the interface, a layering in the liquid phase can be seen for the three systems extending at most up to three or four layers with an exponential decay moving away from the interface. The correlation length for the decay is larger for Fe/Pb than for Fe/Bi or Fe/Zn, indicating a deeper influence for Pb at the Fe(013) interface. This layering is typical of the one found in atomistic studies of solid-liquid interfaces [33]. The liquid structure transition from a statistically average ordered state near the Fe surface to an amorphous structure further away. This implies that the chemical potential of the LM varies within a band fixed by the liquid state difference compared with the solid state and its exact value remains unknown.

4.3. Solid-liquid surface energies and wettability

Fig. 3 presents the calculation of solid-liquid surface energies as a function of the LM chemical potential variation ($\Delta\mu_{LM}=\mu_{Bulk}-\mu_{LM}$) for the Fe(013)/Pb, Fe(013)/Bi and Fe(013)/Zn interfaces. The chemical potential scale is limited to the relevant scale between the LM chemical potential defined by the liquid state and the chemical potential defined by the solid ground state (see Table 2). Note that the interval for the chemical potential is restricted to these physical states of the LM species instead of being taken arbitrarily large like in some prior studies [24].

The projected density of state is plotted in Fig. 4a–c for three interfaces (respectively, Fe/Pb, Fe/Bi and Fe/Zn) for bulk and interfacial atoms. The density of state is broadened for Fe at the interface in the three couples (plotted in red), while there is a noticeable hybridization of the liquid metals d bands with Fe (plotted in blue). Fe majority spin

DOS at Fe/Zn interface are shifted to higher energy than those at Fe/Bi and Fe/Pb interfaces (Fig. 4-d).

The charge density difference is defined by the following:

$$\rho_{diff}(x,y,z) = \rho_{Fe(013)/LM}(x,y,z) - \rho_{LM}(x,y,z) - \rho_{Fe(013)}(x,y,z) \quad (6)$$

The charge-density difference plots for the three interfaces are shown in Fig. 5. There is a charge accumulation (in yellow) on the liquid side of the first layer of adsorbed Pb and Bi. This indicates that there is some degree of charge transfer across the interface in these two cases. For the Fe/Zn interface, there is more charge depletion (in cyan) from Fe than in the Fe/Pb or Fe/Bi cases, agreeing with Fe PDOS. No charge accumulation (yellow) is observed on the other side of Zn, unlike Pb and Bi. This is largely responsible for the larger drop in surface energy in contact with Zn than with Pb or Bi. The charge transfer remains contained in the interface plane for that Fe surface orientation.

5. Discussion

In immiscible systems, such as Fe/Pb or Fe/Bi with partial wetting behavior, liquid inclusions will be expelled from solid solution after elaboration as droplets at GB after processing or heat treatment. There will be a triple junction characterized by a dihedral angle, so that at equilibrium one can infer the ratio of grain boundary interfacial energy relative to the solid-liquid surface energy by:

$$\gamma_{GB} = 2\gamma_{SL}\cos\left(\frac{\theta}{2}\right) \quad (7)$$

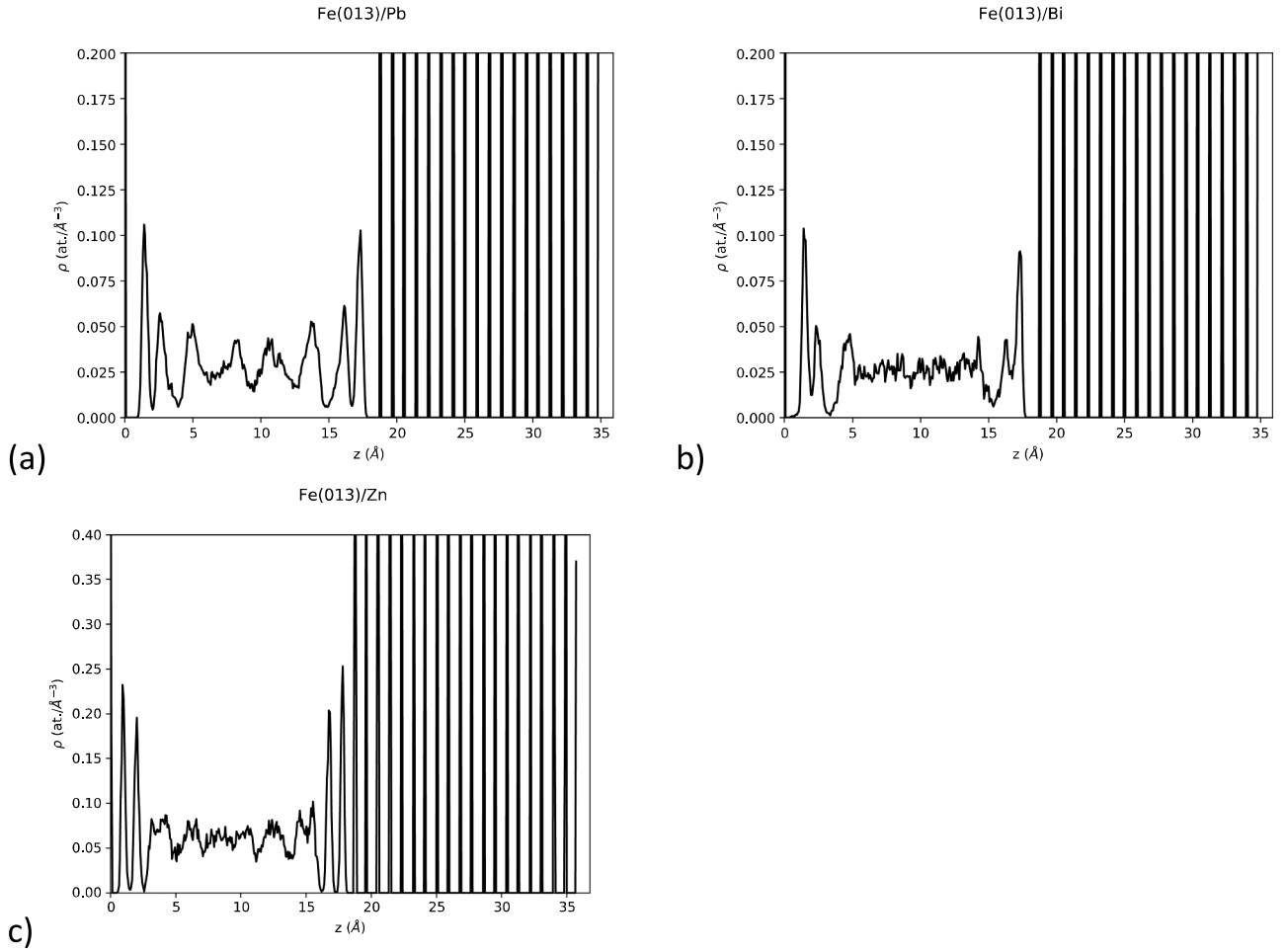Provided that one can exclude liquid species diffusion at the GB and

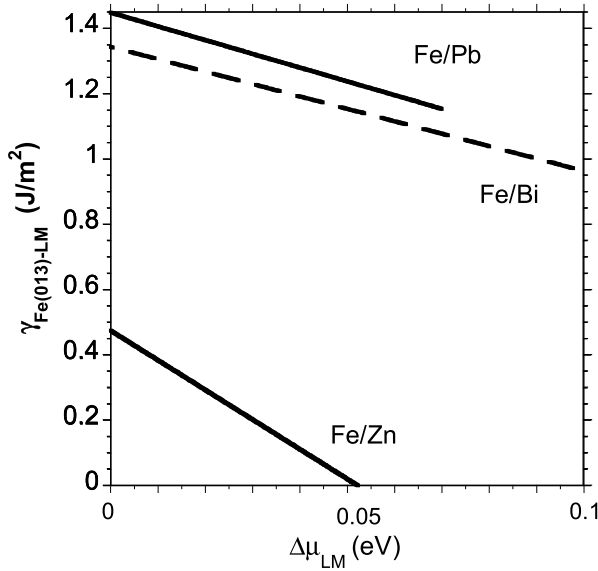**Fig. 2.** Fe(013)-projected density along [1–30] of AIMD at 1000 K: (a) Fe/Pb; (b) Fe/Bi; (c) Fe/Zn.

Fig. 3. Fe(013)/LM interfacial solid-liquid energy (a) $\gamma_{Fe/Pb}$ as a function of Pb chemical potential variation; (b) $\gamma_{Fe/Bi}$ as a function of Bi chemical potential variation (dashed); and (c) $\gamma_{Fe/Zn}$ as a function of Zn chemical potential variation.

treat the GB as a pure iron GB, one could characterize the energy of each grain boundary investigated using for example the recently fitted GB energy function [36]. However, as a way to short cut such a detailed analysis requiring a full determination of the GB five dimensional parameters, we will work using the mean value of a "statistical" approach. Two techniques are possible: the venerable zero-creep technique used by Roth to estimate the mean value of GB energy giving $\langle \gamma_{GB} \rangle = 0.985 \pm 0.05 \ J/m^2$ [37]. A more recent technique, requiring a complete reconstruction of the GB energy function adjusted on atomistic calculations, gives a mean value of $\langle \gamma_{GB} \rangle = 1.11 \pm 0.209 \ J/m^2$ [36,38]. The agreement is deemed fortuitous by the latter authors and caution should certainly be in order there. It neglects, in particular, the fact that in bcc materials, general GBs are not the most frequent because of the strong experimental inverse correlation between the GB energy and its incidence [39]. It seems, however, adequate in a statistical sense for giving the mean value of general GBs and, being interested only qualitatively in a comparison of AIMD results with experimental data, we will then simply use the zero-creep technique estimate in what follows.

The dihedral angles measured in this work for Fe/Bi and in [7] for Fe/Pb, as well as the inferred solid-liquid interfacial energies (γ_{SL}) using the mean GB energy are reported in Table 3 (with error bars whenever possible). The upper value derived from GBW is also reported for Fe/Zn. The ranges of solid-liquid interfacial energies (γ_{SL}) estimated by our AIMD results on Fe(013) are summarized for comparison.

The set of data of measured dihedral angle at GBs underlines that, for example, in the case of Fe/Zn, it would be impossible to rely on experimental wetting studies to quantitatively analyze this couple. Only an upper value can be derived from GBW in accordance however with the
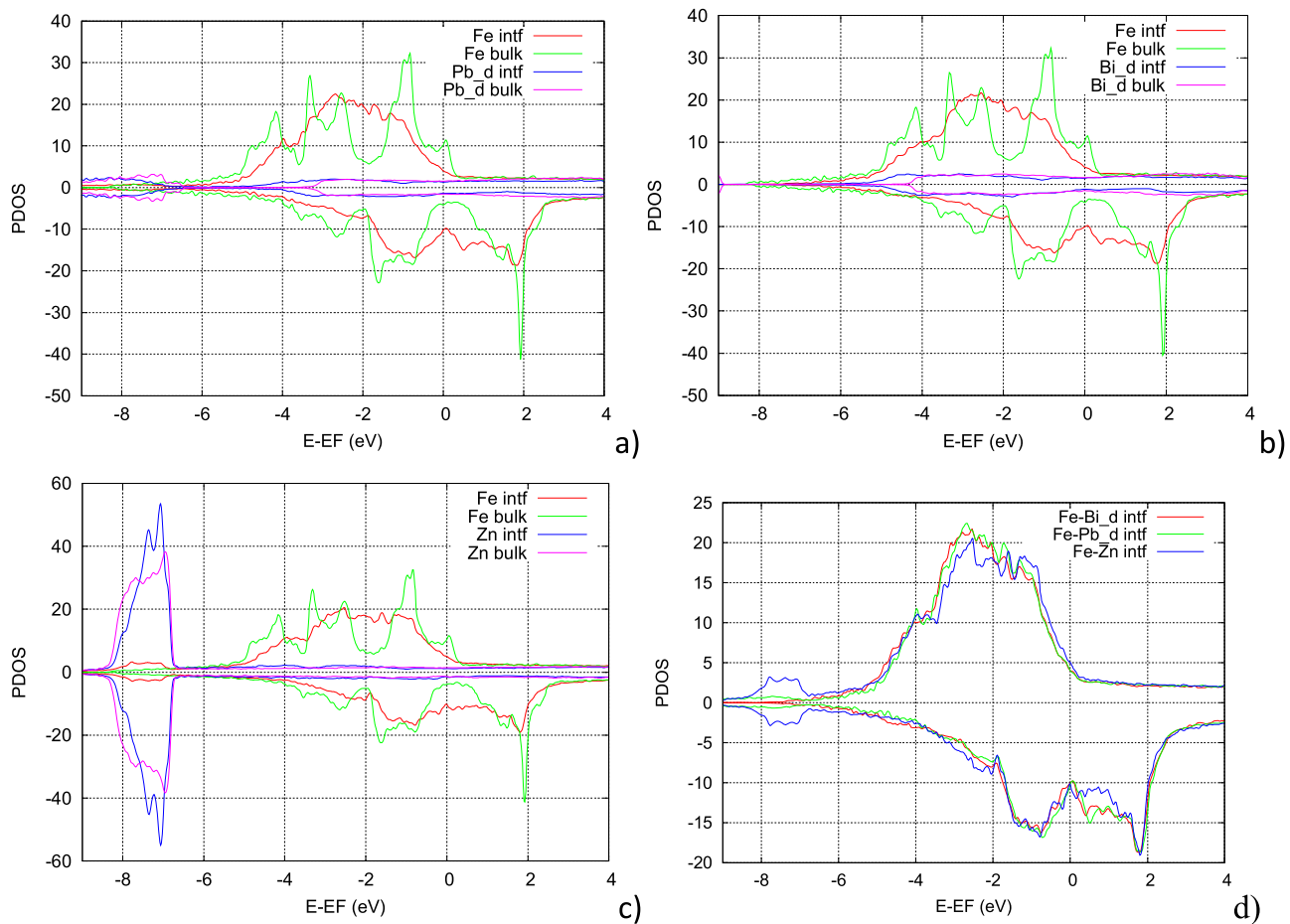
Fig. 4. Bulk and interfacial projected density of states (PDOS): (a) Fe/Pb; (b) Fe/Bi; (c) Fe/Zn; (d) Fe at interfaces. (color online).
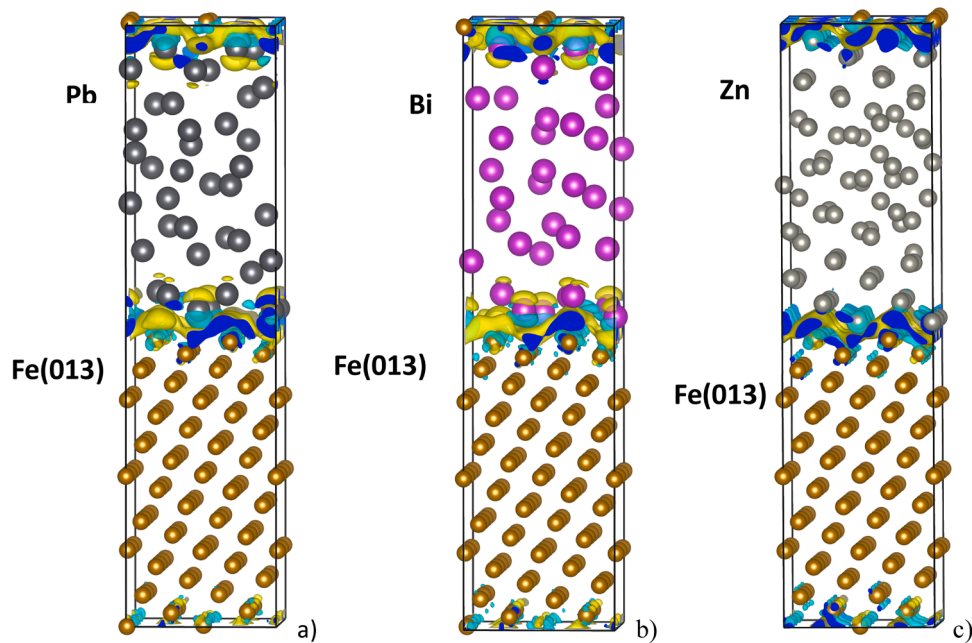
Fig. 5. Fe(013) charge-density difference (iso-surface at ±0.003 e/Å^3): (a) Fe/Pb; (b) Fe/Bi; (c) Fe/Zn with charge accumulation (*depletion*) in yellow (*cyan*), generated using Vesta [35]. (color online).

Miedema's phenomenological estimate of the solid-liquid interface energy for Fe/Zn, which reads $\gamma_{SL}^{Fe/Zn} \approx 0.3 \pm 0.1 \frac{J}{m^2}$ [34]. First, note that the DFT-based estimate of γ_{SL} satisfies the constraint given by the dihedral measurements and, therefore, is into the lower range able to explain GBW from an energetical point of view (provided γ_{SL} is not strongly dependent upon orientation). The Miedema's estimate is also at the correct order of magnitude as well.

For Fe/Pb, using annealed Fe/Pb sintered powder samples, the Fe/Pb interfacial energy is evaluated by the dihedral angle technique at $\gamma_{SL}^{Fe/Pb} \approx 1.2 \frac{J}{m^2}$ [13]. It is higher than the Miedema's estimate by 60 % but well within the range of our estimate for the Fe(013)/Pb interface by a DFT-GGA-PBE type calculation. In view of the limitations of the methodology for deriving the mean GB energy, one can simply conclude that the correct order of magnitude is found here for $\gamma_{SL}^{Fe/Pb}$.

For Fe/Bi, new experiments are reported here for a measurement of the dihedral wetting angle at a triple junction. In spite of being based on a limited set of data (three bismuth inclusions have been analyzed), it shows a surprising small variance of the dihedral angles. The extracted estimate for $\gamma_{SL}^{Fe/Bi}$ is smaller than the lower range of our calculation by GGA-PBE by around 20 % only. Here, one can conclude that the correct order of magnitude is found here for $\gamma_{SL}^{Fe/Bi}$. To explain the 20 % discrepancy, one should note that no bismuth was detected in the GB ahead of the triple junction, so that no GB energy change by intergranular diffusion of Bi species is considered here. Instead, it may have been induced by the GB type that was uncovered during ion-beam machining because it could have a higher energy than the mean value we take. We note that a 10° increase in the dihedral angle brings $\gamma_{SL}^{Fe/Bi}$ into the correct range. So clearly, more statistics would be needed to disprove our approach using this small discrepancy with our modelling. The Miedema's estimate for $\gamma_{SL}^{Fe/Bi}$ is closer to the experimentally inferred one than the DFT estimate.

The wettability parameter S is computed for the relevant range of chemical potential for each LM species (Fig. 6). The Fe-Σ5[100](013) GB energy is taken at 1.43 J/m^2 (details in supplementary). One can see that spontaneous grain-boundary wetting by Bi or Pb is not favored based on this energetic criterion within the entire range of chemical potential to consider, whereas the wettability parameter changes sign in the Fe/Zn case. Therefore, GGA-PBE clearly predicts a change in behavior for a Σ5 [100](013) tilt GB in contact with Zn. The margin for the prediction is quite high in the latter case (more than 0.6 J/m^2), indicating that the prediction is robust against GGA-PBE related inaccuracies to describe the three systems of this study. Zn segregation at grain boundary would lead to a decrease in GB interface energy [24]. With a coverage reaching 1, the GB energy drops by 10 % for the Σ5[100] in Bauer's work. Using the classical wettability parameter S (Eq. (1)), one sees that prior Zn segregation would not change the wettability trend for this GB in contact with Zn since the balance would still largely favor evolving towards a solid-liquid layer.

Considered all together, our predictions for GBW for the three systems match nicely experiment. Recall that no intergranular film has been observed in Fe/Pb or Fe/Bi in unstressed samples, whereas an intergranular film of Zn was consistently observed in a 43° [100] tilt Fe-5at%Si GB [6], as well as in a 38° [100] tilt Fe-6at%Si GB (~Σ5) [27,34], and recently in a Fe-4at%Al Σ5(013)[100] GB [41] among others (Table 1).

6. Conclusion

Ab-initio Molecular Dynamics (AIMD) performed using DFT methods of solid-liquid interfaces predict spontaneous GBW for Fe/Zn but not for Fe/Bi nor Fe/Pb, in good agreement with experiment. This indicates that an AIMD approach is able to capture essential traits of the GB wetting process. This striking agreement with experiment opens the way to predictive schemes in GB wetting and will help current efforts to
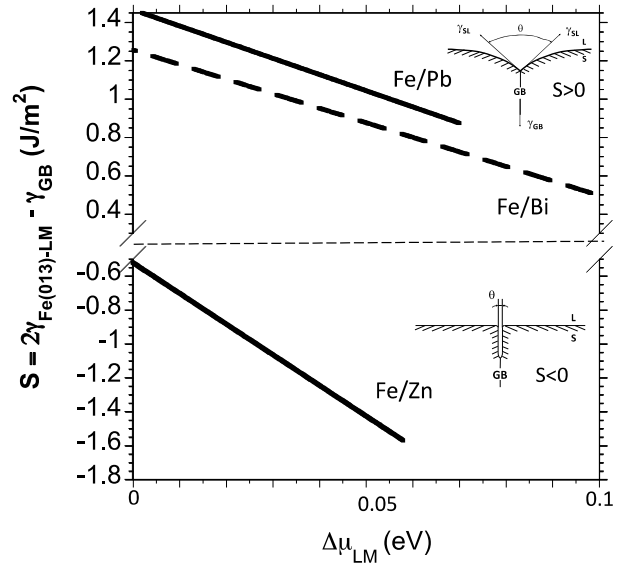

Fig. 6. Grain-boundary wettability parameter for Fe-Σ5(013)/Pb, Fe-Σ5(013)/Bi (dashed line) and Fe-Σ5(013)/Zn as a function of chemical potential variation.

Table 1
Ground states found for the elements Fe, Pb, Bi and Zn by DFT-GGA-PBE.

	Ground state (Pearson)	DFT Cell parameter (nm)	Cohesive energy (eV/atom)	magnetic moment (μ_B)
Fe	cI2	0.283	5.08	2.19
Pb	cF4	0.504	2.954	–
Bi	hR2	0.481 (d$_1$/d$_2$=1.14;α=57.42°)	2.523	–
Zn	hP2	0.264 (a/c = 1.94)	1.097	–

Table 2
Chemical potential μ for each metal as a function of the configuration, with electronic uncertainty (i.e., not statistical) provided.

μ (eV/atom)	Pb	Bi	Zn
μ$_s$, solid bulk (ground state)	−3.565 (+/−0.001)	−3.883 (+/−0.001)	−1.108 (+/−0.001)
μ$_L$, liquid (amorphous)	−3.5078 (+/−0.0005)	−3.781 (+/−0.0002)	- 1.0565 (+/−0.0005)
Final pressure (kBar)	0.92	−2.4	−0.23
ΔH$_{fusion}$ (kJ/mol)	5.8	9.84	4.97
Experimental ΔH$_{fusion}$ (kJ/mol) [31,32]	4.78	11.14	7.07

Table 3
Summary of experimental measurements, Miedema's estimates or AIMD results for GBW wetting and solid-liquid interfacial energies for PB, Bi and Zn.

	Pb	Bi	Zn
Dihedral angle θ (°)	135 ± 10	102	0
Experimentally-inferred γ_{SL} (J/m^2)	1.2 $^{+0.4}_{-0.15}$	0.73	<0.49
Miedema γ_{SL} (J/m^2) from [39]	0.75 (T/T$_f$=1.45)	0.67 (T/T$_f$=1.14)	0.3 ± 0.1[a] (T/T$_f$=1.26)
DFT γ_{SL} (J/m^2)	[1.15, 1.48]	[0.92, 1.35]	[0, 0.48]

[a] For Fe(−5 %Si)/Zn, it was extrapolated in [34] from the Miedema parametrization derived in [40].

mitigate these issues [41,42].

Declaration of Competing Interest

The authors declare that they have no known competing financial interests or personal relationships that could have appeared to influence the work reported in this paper.

Acknowledgments

Supplementary materials

Supplementary material associated with this article can be found, in the online version, at doi:10.1016/j.actamat.2023.119635.

References

[1] B. Straumal, B. Baretzky, Grain boundary phase transitions and their influence on properties of polycrystals, Interface Sci. 12 (2004) 147–155.

[2] B. Bian, S. Taheriniya, G.M. Muralikrishna, A. Godha, S.K. Makineni, S. Sankaran, B.B. Straumal, Y. Du, G. Wilde, S.V. Divinski, Kinetic and structural insights into the grain boundary phase transitions in Ni-Bi alloys, Acta Mater. 245 (2023), 118632.

[3] J. Luo, H. Cheng, K.M. Asl, C.J. Kiely, M.P. Harmer, The role of a bilayer interfacial phase on liquid metal embrittlement, Science 333 (2011) 1730–1733.

[4] R.C. Hugo, R.G. Hoagland, The kinetics of gallium penetration into aluminum grain boundaries–in situ TEM observations and atomistic models, Acta Mater. 48 (2000) 1949–1957.

[5] K. Wolski, V. Laporte, Grain boundary diffusion and wetting in the analysis of intergranular penetration, Mater. Sci. Eng. A 495 (2008) 138–146.

[6] E.I. Rabkin, V.N. Semenov, L.S. Shvindlerman, B.B. Straumal, Penetration of tin and zinc along tilt grain boundaries 43° [100]in Fe-5 at.% Si alloy: premelting phase transition? Acta Metall. Mater. 39 (1991) 627–639.

[7] J.P. Monchoux, E. Rabkin, Microstructure evolution and interfacial properties in the Fe–Pb system, Acta Mater. 50 (2002) 3159–3174.

[8] D.G. Kolman, A review of recent advances in the understanding of liquid metal embrittlement, Corrosion 75 (2019) 42–57.

[9] P.G. De Gennes, Wetting: statics and dynamics, Rev. Mod. Phys. 57 (1985) 827–863.

[10] M. Benhassine, E. Saiz, A.P. Tomsia, J. De Coninck, Nonreactive spreading at high-temperature revisited for metal systems via molecular dynamics, Langmuir 25 (2009) 11450–11458.

[11] M.C. Roth, G.C. Weatherly, W.A. Miller, The temperature dependence of the mechanical properties of aluminum alloys containing low-melting-point inclusions, Acta Metall. 28 (1980) 841–853.

[12] J. Hafner, W. Jank, Structural and electronic properties of the liquid polyvalent elements. IV. The pentavalent semimetals and trends across the periodic table, Phys. Rev. B 45 (1992) 2739–2749.

[13] G. Kresse, Ab initio molecular dynamics: recent progresses and limitations, J. Non-Cryst. Solids 312–314 (2002) 52–59.

[14] J. Souto, M.M.G. Alemany, L.J. Gallego, L.E. González, D.J. González, Ab initio molecular dynamics study of the static, dynamic, and electronic properties of liquid Bi near melting using real-space pseudopotentials, Phys. Rev. B 81 (2010), 134201.

[15] M. Davidović, M. Stojić, D.J. Jović, Disordered structure of molten monatomic metals, semimetals and semiconductor, J. Non-Cryst. Solids 61-62 (1984) 517–522.

[16] M. Mayo, E. Yahel, Y. Greenberg, G. Makov, Short range order in liquid pnictides, J. Phys. Condens. Matter 25 (2013), 505102.

[17] I.G. Dmukhovskaya, V.V. Popovich, Effect of lead on the fracture of Armco iron, Sov. Mater. Sci. Transl. Fiz. Khimicheskaya Mekhanika Mater./Acad. Sci. Ukr. SSR 15 (1980) 366–369.

[18] P.E. Blöchl, Projector augmented-wave method, Phys. Rev. B 50 (1994) 17953.

[19] G. Kresse, J. Furthmüller, Efficiency of ab-initio total energy calculations for metals and semiconductors using a plane-wave basis set, Comput. Mater. Sci. 6 (1996) 15–50.

[20] G. Kresse, J. Furthmüller, Efficient iterative schemes for ab initio total-energy calculations using a plane-wave basis set, Phys. Rev. B 54 (1996) 11169.

[21] J.P. Perdew, K. Burke, M. Ernzerhof, Generalized gradient approximation made simple, Phys. Rev. Lett. 77 (1996) 3865.

[22] H.J. Monkhorst, J.D. Pack, Special points for Brillouin-zone integrations, Phys. Rev. B 13 (1976) 5188–5192.

[23] M. Methfessel, A.T. Paxton, High-precision sampling for Brillouin-zone integration in metals, Phys. Rev. B 40 (1989) 3616.

[24] K.D. Bauer, M. Todorova, K. Hingerl, J. Neugebauer, A first principles investigation of zinc induced embrittlement at grain boundaries in bcc iron, Acta Mater. 90 (2015) 69–76.

[25] X. Gonze, J.P. Michenaud, J.P. Vigneron, First-principles study of As, Sb, and Bi electronic properties, Phys. Rev. B 41 (1990) 11827.

[26] K. Lejaeghere, V. Van Speybroeck, G. Van Oost, S. Cottenier, Error estimates for solid-state density-functional theory predictions: an overview by means of the ground-state elemental crystals, Crit. Rev. Solid State Mater. Sci. 39 (2014) 1–24.

[27] B. Straumal, E. Rabkin, W. Lojkowski, W. Gust, L.S. Shvindlerman, Pressure influence on the grain boundary wetting phase transition in Fe-Si alloys, Acta Mater. 45 (1997) 1931–1940.

[28] M.L. Martin, T. Auger, D.D. Johnson, I.M. Robertson, Liquid-metal-induced fracture mode of martensitic T91 steels, J. Nucl. Mater. 426 (2012) 71–77.

[29] U. Dahlborg, M. Davidovič, On the structure of liquid bismuth, Phys. Chem. Liq. 15 (1986) 243–252.

[30] Y. Waseda, The Structure of Non-Crystalline Materials: Liquids and Amorphous Solids, McGraw-Hill International Book Co., New York, 1980.

[31] S. Stølen, F. Grønvold, Critical assessment of the enthalpy of fusion of metals used as enthalpy standards at moderate to high temperatures, Thermochim. Acta 327 (1999) 1–32.

[32] R.M. Brugger, R.B. Bennion, T.G. Worlton, The crystal structure of bismuth-II at 26 kbar, Phys. Lett. A 24 (1967) 714–717.

[33] P. Geysermans, D. Gorse, V. Pontikis, Molecular dynamics study of the solid–liquid interface, J. Chem. Phys. 113 (2000) 6382–6389.

[34] W. Lojkowski, E. Rabkin, B.B. Straumal, W. Gust, Excess volume of the solid/liquid interface in Fe-6 at.%Si bicrystals wetted by liquid zinc, Interface Sci. 6 (1998) 179–186.

[35] K. Momma, F. Izumi, VESTA 3 for three-dimensional visualization of crystal, volumetric and morphology data, J. Appl. Crystallogr. 44 (2011) 1272–1276.

[36] R. Sarochawikasit, C. Wang, P. Kumam, H. Beladi, T. Okita, G.S. Rohrer, S. Ratanaphan, Grain boundary energy function for α iron, Materialia 19 (2021), 101186.

[37] T.A. Roth, The surface and grain boundary energies of iron, cobalt and nickel, Mater. Sci. Eng. 18 (1975) 183–192.

[38] S. Ratanaphan, D.L. Olmsted, V.V. Bulatov, E.A. Holm, A.D. Rollett, G.S. Rohrer, Grain boundary energies in body-centered cubic metals, Acta Mater. 88 (2015) 346–354.

[39] H. Beladi, G.S. Rohrer, The relative grain boundary area and energy distributions in a ferritic steel determined from three-dimensional electron backscatter diffraction maps, Acta Mater. 61 (2013) 1404–1412.

[40] A.R. Miedema, F.J.A. den Broeder, On the interfacial energy in solid-liquid and solid-solid metal combinations, Z. Metallkd. 70 (1979) 14–20.

[41] A. Ahmadian, D. Scheiber, X. Zhou, B. Gault, L. Romaner, R.D. Kamachali, W. Ecker, G. Dehm, C.H. Liebscher, Interstitial Segregation has the Potential to Mitigate Liquid Metal Embrittlement in Iron, Adv. Mater. 35 (2023), 2211796.

[42] D. Scheiber, K. Prabitz, L. Romaner, W. Ecker, The influence of alloying on Zn liquid metal embrittlement in steels, Acta Mater. 195 (2020) 750–760.